

Supporting Information

Thermoelectric Nanowires for Dense 3D Printed Architectures

Danwei Zhang^{*a}, *Jayanthi Ramiah*^{a,b}, *Mehmet Cagirici*^c, *Kivanc Saglik*^{a,d}, *Samantha Faye Duran Solco*^a, *Jing Cao*^{*a}, *Jianwei Xu*^{*a,e}, *Ady Suwardi*^{*a,f}

- a. Institute of Materials Research and Engineering, Agency for Science, Technology and Research (A*STAR), Singapore 138634.
- b. School of Chemistry, The University of Sydney, Camperdown NSW 2050, Australia.
- c. Singapore Centre for 3D Printing, Nanyang Technological University, 65 Nanyang Drive, Singapore 639798.
- d. School of Materials Science and Engineering, College of Engineering, Nanyang Technological University, Singapore 639798.
- e. Institute of Sustainability for Chemicals, Energy and Environment, Agency for Science, Technology and Research (A*STAR), Singapore 627833.
- f. Department of Materials Science and Engineering, College of Design and Engineering, National University of Singapore, Singapore 117575.

Corresponding to: zhang_danwei@imre.a-star.edu.sg; cao_jing@imre.a-star.edu.sg;
xu_jianwei@isce2.a-star.edu.sg; ady_suwardi@imre.a-star.edu.sg

Methods

Ink Preparation

Materials. Tellurium dioxide (TeO_2 , 99.995%) powder, polyvinyl pyrrolidone (PVP, $M_w = 40\,000$), ethylene glycol (EG), bismuth nitrate pentahydrate ($\text{Bi}(\text{NO}_3)_3 \cdot 5\text{H}_2\text{O}$, $\geq 99.99\%$), sodium hydroxide (NaOH) and hydrazine hydrate were purchased from Sigma-Aldrich, Singapore and used as received. Dimethyl sulfoxide (DMSO) was purchased from Kanto Chemical, Japan.

Synthesis of Bi_2Te_3 Nanowires. The fabrication of Bi_2Te_3 nanowires is adapted and modified according to the polyol process reported by Zhang and colleagues.¹ The synthesis of Bi_2Te_3 nanowires was carried out in the presence of NaOH and performed accordingly: PVP (2 g), TeO_2 (4.79 g) and NaOH (6.0 g) were added to EG (200 ml) in a 500 mL three-necked round bottom flask with continuous magnetic stirring at 500 rpm. After the temperature had stabilized at 160°C , hydrazine (6 ml) was injected into the solution. 9.7g of $\text{Bi}(\text{NO}_3)_3 \cdot 5\text{H}_2\text{O}$ was dissolved in 50 ml of EG and injected drop-wise into the Te nanowire solution. The reaction was left to stir for a further 4 h at a constant temperature of 160°C . The solution was then left to cool down to room temperature. The final products were obtained by centrifugation at 14000 rpm (22830 x g), followed by washing with ethanol (99%) several times until a clear supernatant was obtained.

Fabrication of 3D Bi_2Te_3 Structures. Bi_2Te_3 nanowires were centrifuged in DMSO for 5 min at 14000 rpm (22830 x g). Excess DMSO was removed to obtain a slurry suitable for 3D printing. The slurry was homogenized in an agate mortar and pestle. 3D Bi_2Te_3 structures were printed using Cellink Bio X, Sweden, 3D Printer using tapered deposition nozzles of varying orifice diameters (0.250mm (25G), 0.410 mm (22G), 0.580 mm (20G)). Air pressures between 100-200 kPa and a printing speed between 5-10 mm s^{-1} were used. The G-code was modified to obtain a similar linear infill pattern in each layer.

Post-printing Heat Treatment. The printed structures were left to dry at ambient room temperature slowly to minimize warpage and cracks. Vacuum drying at elevated temperatures can also be used to accelerate the drying process. The BTNW green body was then subjected to residual DMSO solvent decomposition and burn-off at 100°C - 150°C for 2 – 5 h, depending on the size of the structure. Densification of BTNW structures was conducted at 450°C for 2h

or 5h. A ramping and cooling rate of $1^{\circ}\text{C min}^{-1}$ was used throughout the heat treatment process to minimize internal stresses for a crack-free structure. Forming gas (95% N_2 - 5% H_2) with a flow of 180 sccm was used.

Characterization

Ink Properties. The rheological properties of the ink were measured by a rotational rheometer (TA Instruments, DHR-3, USA) with 25 mm aluminum parallel plates. The flow ramp tests were conducted over a shear rate of 0.01 to 200 s^{-1} and immediately back to 0.01 s^{-1} . The angular frequency tests were carried out from 0.1 to 500 rad s^{-1} at a constant stress of 10 Pa. The modulus test was conducted over a range of 1 Pa till yield point at an angular frequency of 10 rad s^{-1} . The rheological measurements were conducted with a $300 \mu\text{m}$ test gap and an environmental temperature of 25°C . Thermal analysis of BTNW ink was conducted using TA Instruments, TGA Q500, USA using a ramp rate of $5^{\circ}\text{C min}^{-1}$ from room temperature to 300°C .

BTNW Microstructure Analysis. The grain morphologies of mechanically polished samples were assessed using Electron Scattered Backscattered Diffraction (EBSD) (JEOL 7600 FESEM equipped with EBSD detector, Japan). A proper step size of $1 \mu\text{m}$ was determined considering the existence of small pores. Although smaller grains were observed in each sample, they were excluded from the grain size analyses. Elemental analysis was also conducted for the sintered BTNW structures using Energy Dispersive Spectroscopy (EDS) (Oxford Instruments, X-Max, UK). Orientation of Bi_2Te_3 nanowires was analyzed using OrientationJ plugin for ImageJ software. X-ray diffraction (XRD) analysis was conducted on both BTNW and sintered BTNW structures using a $\text{Cu K}\alpha$ source (1.5418 \AA) (Bruker D8 Advance, Germany). The samples were scanned over a range from 20° to 80° in an increment of 0.02° with a time step of 0.5 s.

BTNW Structure Thermoelectric Properties. Electrical conductivity and Seebeck Coefficient data were measured within a temperature range of 30°C to 190°C under Helium atmosphere using an ULVAC ZEM-3 thermoelectric measurement system. Thermal diffusivity D was measured using a laser flash method (NETZSCH LFA 457, Germany) in the temperature range of 30°C to 190°C . Thermal conductivity can be calculated based on the relationship $\kappa = \rho C_p D$, where ρ is the density, C_p is the specific heat capacity and D is the thermal diffusivity. Density

ρ was measured using a home-built Archimedes density measurement setup. Specific heat capacity C_p was estimated using the Dulong-Petit Law.

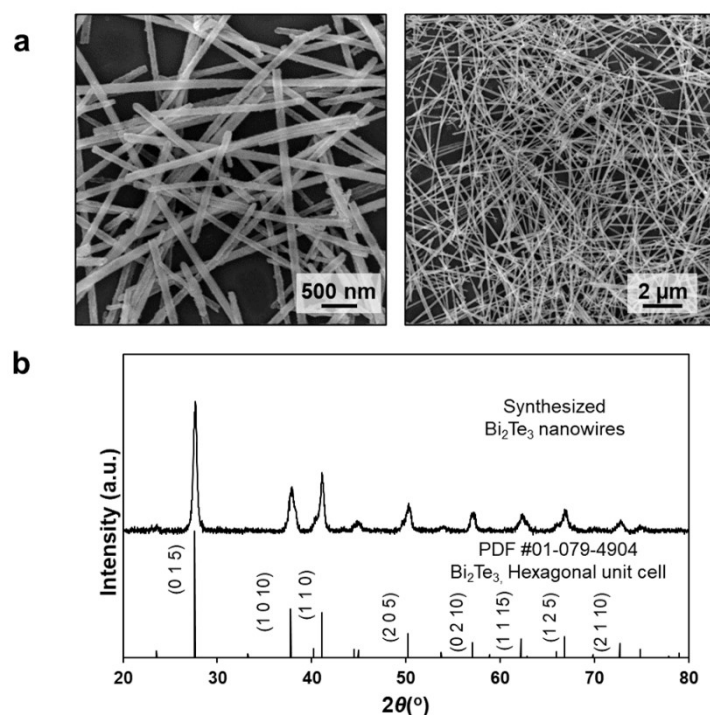


Fig. S1. Synthesized Bi_2Te_3 nanowires. (a) SEM images of synthesized Bi_2Te_3 nanowires and (b) XRD analysis of synthesized Bi_2Te_3 nanowires match PDF #01-079-4904 of Bi_2Te_3 with hexagonal unit cell.

The morphology of solution-synthesized Bi_2Te_3 nanowires was analyzed using scanning electron microscopy (SEM). SEM images of fabricated nanowires are shown in **Fig. S1a**. The synthesized nanowires have an aspect ratio, s , of approximately 176 with an average length (l) of $6.80 \pm 1.26 \mu\text{m}$ and diameter (d) of $38.6 \pm 4.9 \text{ nm}$. The composition and phase of the synthesized products were examined via X-ray diffraction (XRD). **Fig. S1b** presents the XRD pattern of the synthesized Bi_2Te_3 nanowires. All diffraction peaks in this pattern were indexed to the Rhombohedral crystal structure of Bi_2Te_3 (PDF #01-079-4904). No noticeable peaks of Te phase were observed.

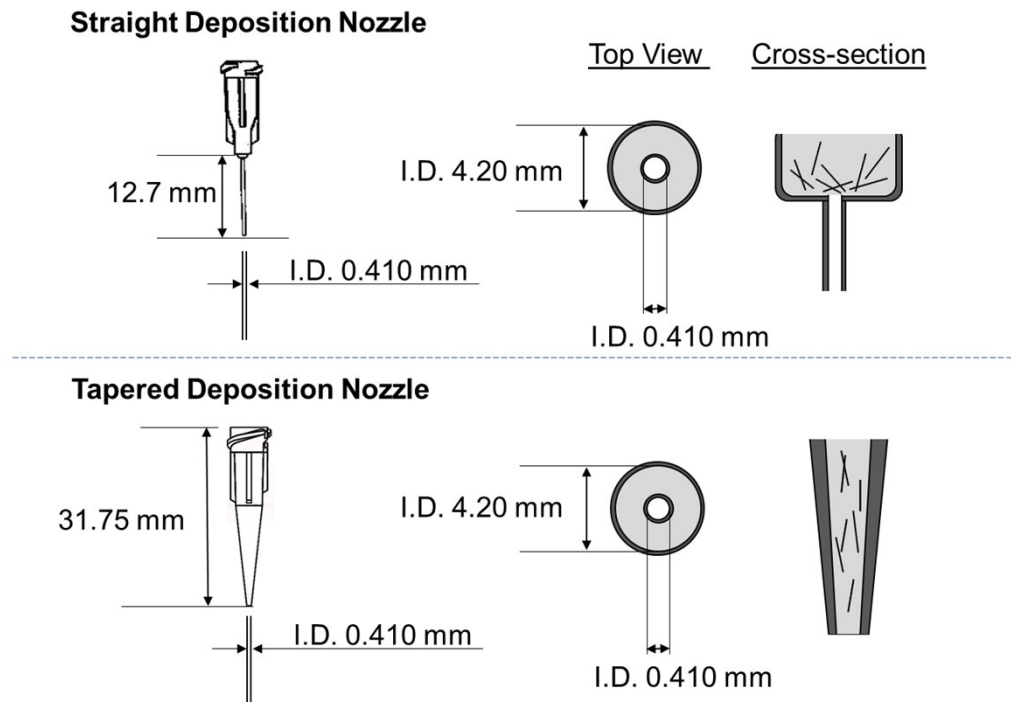


Fig. S2. Comparison of straight deposition nozzles and tapered deposition nozzles for fiber alignment.

Shear-induced fiber alignment through direct ink writing has been reported by several groups for applications for microwave attenuation² and in sustainable lightweight composites³⁻⁵. In our application, a high concentration of nanowires is needed to allow for subsequent dense sintered thermoelectric structures. With a high concentration of nanowires, the nozzle geometry is important in ensuring a successful continuous print. As compared to tapered nozzles, clogging will be more probable in straight deposition nozzles due to the accumulation of misorientated fibers with the step-like reduction at the nozzle tip as studied by Croom and colleagues⁶ (see **Fig. S2**). Thus, tapered nozzles were chosen as the preferred nozzle for highly concentrated fiber ink during extrusion.

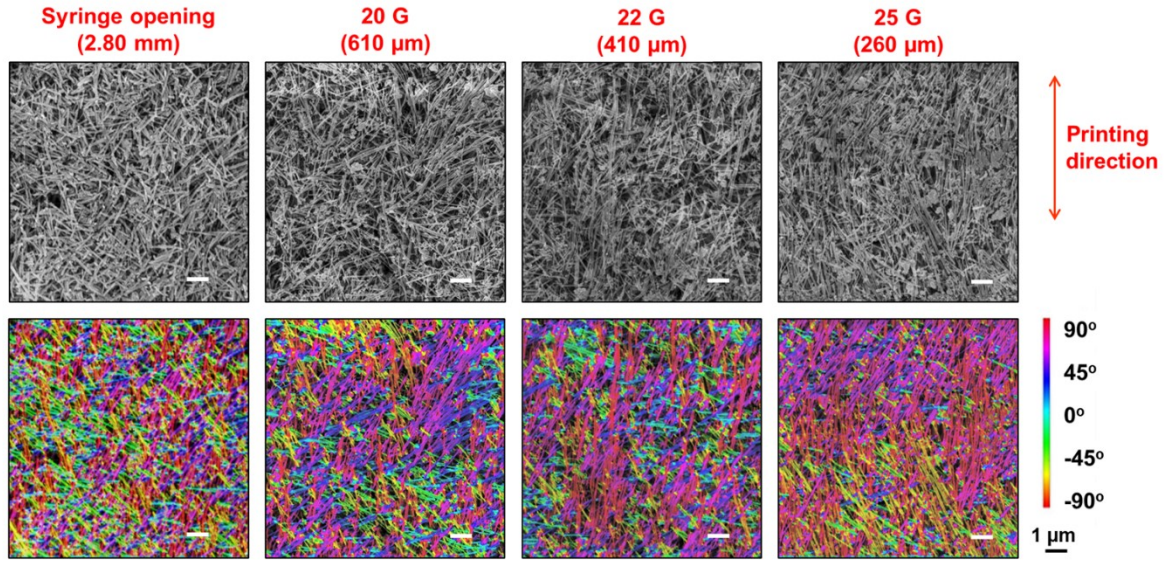


Fig. S3. Effects of nozzle radius on nanowire alignment. When extruded through different nozzle sizes, the Bi_2Te_3 nanowire ink system experiences both shear and extensional flow. Scale = 1 μm .

At the syringe exit, there is a random alignment of the nanowires. As it passes through various-sized tapered nozzles, the nanowires begin to align. For inks extruded through tapered nozzles, the ink experiences both shear and extensional flow for particle alignment. Shear-induced alignment is experienced by the ink near the skin of the printed filament while extensional flow is experienced throughout the capillary length which has a higher effect on aligning the particles efficiently.^{7,8} In maintaining structural fidelity, the smaller the radius of nozzle, the higher the pressure needed for extrusion. This can be examined by the flow of ink through a capillary in **Equation S1** below:⁹

$$\tau_r = \frac{r\Delta P}{2l} \quad (\text{S1})$$

Where the radially varying shear stress (τ_r) experienced by the ink is dependent on the pressure gradient ΔP is applied along the capillary length (l) and r is the radial position within the nozzle (i.e., $r = 0$ at the center axis and $r = R$ at the nozzle wall).

Therefore, using a smaller nozzle of 25G (260 μm) nozzle (smaller r), the BTNW ink experiences higher shear stress, thus allowing for greater particle alignment as compared to 20G (610 μm)

and 22G (410 μm) nozzles (see **Fig. S3**). However, a smaller nozzle would require a longer print time as compared to a larger nozzle. The probability of clogged nozzles would also be greater. Therefore, in our work, 22G (410 μm) nozzles were used.

Table S1. Comparison Table of the Filler-derived Density Index (FDI) of 3D printed Bi₂Te₃-based structures

Filler Material	3D Printing Method	Filler Material (wt%)	Sintering Aid	Sintering Temperature – Dwelling Duration	Density of sintered part	FDI	Ref.
<i>Adding chalcogenidometallate (ChaM) binder as sintering aid</i>							
BiSbTe	DIW	55.6	25 wt% Sb ₂ Te ₄	450°C – 2 hours	75-80%	1.44	¹⁰
Bi _{0.5} Sb _{1.5} Te ₃	DIW	62.5	25 wt% Sb ₂ Te ₃	450°C – 1 hours	58%	0.92	¹¹
Bi _{0.55} Sb _{1.45} Te ₃ ,	DIW	55.5,	25 wt% Sb ₂ Te ₄ ,	450°C – 30 min	82 %,	1.48	¹²
Bi ₂ Te _{2.7} Se _{0.3}		48.9	10 wt% Sb ₂ Te ₄		72 %	1.47	
<i>Adding elemental powders as sintering aid</i>							
Bi _{0.4} Sb _{1.6} Te ₃ ,	DIW	~89,	7% Te,	500°C – 4 hours	~78,	0.88,	¹³
Bi ₂ Te _{2.6} Se _{0.4}		~89	10% Se		~80%	0.90	
<i>No addition of sintering aid</i>							
Bi _{0.5} Sb _{1.5} Te ₃ ,	DIW	91,	-	450°C – 6 hours	~70%,	0.77,	¹⁴
Bi ₂ Te ₃		91			~64.6%	0.71	
Bi _{0.5} Sb _{1.5} Te ₃ ,	DIW	74,	-	450°C – 2 hours	68.2%,	0.92,	¹⁵
Bi ₂ Te _{2.7} Se _{0.3}		74			80.7%	1.09	
Bi₂Te₃ nanowires	DIW	32.3	-	450°C – 2 hours	81.1 %	2.51	This work

The Filler-derived Density Index (FDI) in Table S1 is calculated according to **Equation 2** (of the main article):

$$FDI = \frac{\text{Density (\% of theoretical density)}}{\text{Base filler material (wt\%) + Sintering aids (wt\%)}} \quad (2)$$

Where the sample's sintered density is calculated as a percentage of the material's theoretical density. The base filler material and sintering aids that contributes to the densification of the sintered material is calculated as their respective weight percentage in the overall ink system.

Table S2. Comparison Table of 3D-printed Bi₂Te₃ thermoelectric structures.

Thermoelectric	Morphology	3D Printing Method	Topology	Flow Behaviour	Density	<i>zT</i>	Ref.
Bi ₂ Te ₃	Nanowire	Ink-Jetting	Planar	Newtonian	-	0.04	¹⁶
Bi ₂ Te ₃	Nanowire	Ink-Jetting	Planar	Newtonian	-	0.25	¹⁷
Bi ₂ Te ₃	Powder	DIW	Vertical	Non-Newtonian Pseudoplastic	~64.6 % (450°C-6h)	0.11	¹⁴
Bi₂Te₃	Nanowire	DIW	Vertical	Non-Newtonian Pseudoplastic	81.1 % (450°C-2h)	0.31	This work

References

1. G. Zhang, B. Kirk, L. A. Jauregui, H. Yang, X. Xu, Y. P. Chen and Y. Wu, *Nano Letters*, 2012, **12**, 56-60.
2. G. J. H. Lim, Z. Yang, Y. Hou, P. J. Sugumaran, Z. Qiao, J. Ding, W. Yan and Y. Yang, *ACS Applied Materials & Interfaces*, 2022, **14**, 31267-31276.
3. G. Siqueira, D. Kokkinis, R. Libanori, M. K. Hausmann, A. S. Gladman, A. Neels, P. Tingaut, T. Zimmermann, J. A. Lewis and A. R. Studart, *Advanced Functional Materials*, 2017, **27**, 1604619.
4. B. G. Compton and J. A. Lewis, *Advanced Materials*, 2014, **26**, 5930-5935.
5. M. Ziaee, J. W. Johnson and M. Yourdkhani, *ACS Applied Materials & Interfaces*, 2022, **14**, 16694-16702.
6. B. P. Croom, A. Abbott, J. W. Kemp, L. Rueschhoff, L. Smieska, A. Woll, S. Stoupin and H. Koerner, *Additive Manufacturing*, 2021, **37**, 101701.
7. M. K. Hausmann, P. A. Rühls, G. Siqueira, J. Läger, R. Libanori, T. Zimmermann and A. R. Studart, *ACS Nano*, 2018, **12**, 6926-6937.
8. A. S. Lubansky, in *Comprehensive Biotechnology (Second Edition)*, ed. M. Moo-Young, Academic Press, Burlington, 2011, DOI: <https://doi.org/10.1016/B978-0-08-088504-9.00528-6>, pp. 189-201.
9. J. E. Smay, J. Cesarano and J. A. Lewis, *Langmuir*, 2002, **18**, 5429-5437.
10. S. E. Yang, F. Kim, F. Ejaz, G. S. Lee, H. Ju, S. Choo, J. Lee, G. Kim, S.-h. Jung, S. Ahn, H. G. Chae, K. T. Kim, B. Kwon and J. S. Son, *Nano Energy*, 2021, **81**, 105638.
11. F. Kim, B. Kwon, Y. Eom, J. E. Lee, S. Park, S. Jo, S. H. Park, B.-S. Kim, H. J. Im, M. H. Lee, T. S. Min, K. T. Kim, H. G. Chae, W. P. King and J. S. Son, *Nature Energy*, 2018, **3**, 301-309.
12. F. Kim, S. E. Yang, H. Ju, S. Choo, J. Lee, G. Kim, S.-h. Jung, S. Kim, C. Cha, K. T. Kim, S. Ahn, H. G. Chae and J. S. Son, *Nature Electronics*, 2021, **4**, 579-587.
13. X. Zhang, J. Chen, H. Zhang, P. Zhu, R. Wang, F. Li and B. Li, *Journal of Materiomics*, 2023, **9**, 328-337.
14. N. Su, P. Zhu, Y. Pan, F. Li and B. Li, *Energy*, 2020, **195**, 116892.
15. Z. Wang, W. Cui, H. Yuan, X. Kang, Z. Zheng, W. Qiu, Q. Hu, J. Tang and X. Cui, *Materials Today Energy*, 2023, **31**, 101206.
16. B. Chen, M. Kruse, B. Xu, R. Tutika, W. Zheng, M. D. Bartlett, Y. Wu and J. C. Claussen, *Nanoscale*, 2019, **11**, 5222-5230.
17. B. Chen, S. R. Das, W. Zheng, B. Zhu, B. Xu, S. Hong, C. Sun, X. Wang, Y. Wu and J. C. Claussen, *Advanced Electronic Materials*, 2017, **3**, 1600524.